Materials Advances

ROYAL SOCIETY OF CHEMISTRY

PAPER

View Article Online
View Journal | View Issue

Cite this: *Mater. Adv.*, 2025, 6, 8936

Facile and green carboxylation of never-dried bacterial cellulose produced from low-cost substrates: structural characterization and copper binding performance

Mohammad Sadegh Jafari,[a] Samaneh Ghadami,[b] Shobha Mantripragada,[b] Kristen Dellinger,[b] Jeffrey R. Alston [b] and Dennis R. LaJeunesse *[a]

Received 8th July 2025,
Accepted 7th October 2025

DOI: 10.1039/d5ma00725a

rsc.li/materials-advances

In this study, bacterial cellulose production was optimized using molasses and cheese whey *via* response surface methodology, a central composite design approach. Using *Gluconacetobacter hansenii*, the effects of sugar, protein, pH, and acetic acid were evaluated, resulting in a 6.85-fold yield increase from 0.9 (HS media) to 6.17 g L^{-1}. The produced BC was hydrolyzed with sulfuric acid to generate bacterial cellulose nanocrystals (BCNC), followed by functionalization through the Fenton reaction to synthesize carboxylated BCNC (BCNC-H). Structural analyses using FTIR and XPS confirmed successful carboxylation, with the O/C ratio increasing from 0.55 (BC) to 0.68 (BCNC-H). Zeta potential measurements demonstrated a significant increase in the absolute negative surface charge (−22.53 mV for BC *vs.* −37.46 mV for BCNC-H). SEM images revealed a substantial reduction in fiber diameter after sulfuric acid treatment and the Fenton reaction (BC > BCNC > BCNC-H). Thermal and crystallinity properties were also evaluated. Finally, BCNC-H exhibited excellent Cu^{2+} adsorption capacity (164 ± 8.07 mg g^{-1}), representing a 173% increase over unmodified BC, highlighting its potential as a sustainable and efficient biopolymer-based adsorbent for water and wastewater treatment.

1. Introduction

Clean drinking water is essential for human civilization. However, rapid population growth has increased the demand for high-quality water. Industrialization and technological advancements have led to the generation of vast amounts of waste, which contaminate the water supply. Of this waste, heavy metals from a variety of industries including mining and semiconductor manufacturing, are among the most dangerous and difficult to clean and detect.[1] Certain heavy metals in small amounts, such as copper (Cu), are essential for biological functions, including enzyme activity and tissue development.[2] At higher concentrations, copper becomes toxic, accumulating in the brain, kidneys, heart, and liver, resulting in symptoms such as vomiting, diarrhea, stomach cramps, nausea, and even death.[3,4] Copper is the third most widely used metal globally and after mercury, the second most toxic element in drinking water.[5,6] Therefore, the development of effective and sustainable methods for copper removal from wastewater is of paramount importance.

Various approaches have been used for copper remediation, including filtration, precipitation, ion exchange, electrochemistry, and solvent extraction.[4] However, the removal of even trace amounts of heavy metals in the solutions using these methods is economically and technically unfeasible. In contrast, adsorption has emerged as a highly promising method due to its simplicity, cost-effectiveness, regenerative ability, and compatibility with low concentrations of non-biodegradable pollutants.[7,8] Cellulose is an excellent material for such applications. With abundant surface hydroxyl groups (–OH) and capacity for chemical modification, regenerative ability, and excellent mechanical strength, cellulose is an ideal candidate for the removal of metals from aqueous solutions.[9,10] Mild treatment of cellulose with sulfuric acid (H_2SO_4) not only produces cellulose nanocrystals (CNCs) with a higher specific surface area but also esterifies surface hydroxyl groups, introducing sulfate groups ($-OSO_3^-$).[11] Cellulose functionalized with these sulfate groups results in a negative surface charge, thereby improving the colloidal stability of the resulting CNCs in the suspension.[12] Oxygen, nitrogen, and sulfur atoms in functional groups such as carboxyl groups (–COOH), amines, and thiols often form strong chelation bonds with heavy metal ions.[13] Consequently, grafting these functional groups onto the

[a] *Department of Nanoscience, Joint School of Nanoscience and Nanoengineering, University of North Carolina Greensboro, Greensboro, North Carolina 27401, USA. E-mail: drlajeun@uncg.edu; Tel: +1 3362852866*
[b] *Department of Nanoengineering, Joint School of Nanoscience and Nanoengineering, North Carolina A&T State University, Greensboro, North Carolina 27401, USA*

cellulose surface can enhance its capacity for metal ion adsorption.[14] Although 2,2,6,6-tetramethylpiperidine-1-oxyl (TEMPO) and ammonium persulfate (APS) are widely employed to introduce these functional groups, both approaches are associated with environmental and technical limitations, such as the generation of toxic byproducts, prolonged reaction durations, and elevated costs.[15,16] In contrast, hydrogen peroxide (H_2O_2) is a greener oxidizing agent that decomposes into water and oxygen, making it more suitable for sustainable applications.

Plant-based cellulose is often accompanied by different kinds of impurities like lignin, hemicellulose, and pectin, and its purification requires chemical processes that may damage its structure or contribute to further environmental pollution.[17] Alternatively, bacterial cellulose (BC) is the purest form of cellulose produced by bacteria such as *Gluconacetobacter hansenii* (*G. hansenii*) and *Gluconacetobacter xylinus*.[18] However, the application of BC is limited due to the high production cost. To address this, cost-effective substrates such as agricultural and dairy by-products have been explored for BC production. Molasses and cheese whey are particularly promising due to their high sugar and protein contents, respectively.[19] Cheese whey, a byproduct rich in lactose and growth factors, is generated in large quantities worldwide, approximately 178.5 billion liters annually, and poses significant environmental risks due to its high chemical and biological oxygen demand (COD, BOD),[20] which can reach up to 40 000 mg L^{-1}.[21] Although *G. hansenii* cannot metabolize lactose, combining molasses and cheese whey provides an effective, low-cost medium with minimal environmental footprint.[22,23] To optimize a medium for a complex biological process influenced by multiple variables, response surface methodology (RSM) offers a more systematic and efficient optimization strategy compared to traditional techniques like the one-factor-at-a-time (OFAT) method.[24] Central composite design (CCD), a form of RSM, allows for the evaluation of multiple parameters and their interactions, providing statistically robust optimization for process conditions.[25]

In this study, BC was produced using *G. hansenii* (ATCC 23769) cultivated in a medium composed of molasses and cheese whey. For the first time, CCD-RSM was applied to optimize BC production in a molasses-cheese whey medium by assessing the effects of total sugar concentration (g L^{-1}), total protein concentration (g L^{-1}), acetic acid (% v/v), and pH. The resulting BC was hydrolyzed with sulfuric acid to obtain BCNCs, which were subsequently carboxylated using the Fenton reaction, a green and sustainable approach, for wet BCNC modification using $FeSO_4 \cdot 7H_2O$ and H_2O_2 to introduce –COOH groups. Based on the available literature, there appears to be no prior investigation into the application of the Fenton reaction to carboxylate wet BCNC. The materials (BC, BCNC, and BCNC-H) were characterized using scanning electron microscopy (SEM), Fourier-transform infrared spectroscopy (FTIR), X-ray diffraction (XRD), and X-ray photoelectron spectroscopy (XPS). Surface charge and thermal properties were evaluated through zeta potential and thermogravimetric analysis (TGA and DTG). Finally, the copper adsorption capacity of BCNC-H was investigated, highlighting its potential as a sustainable, high-performance adsorbent for heavy metal remediation in contaminated water systems (Fig. 1).

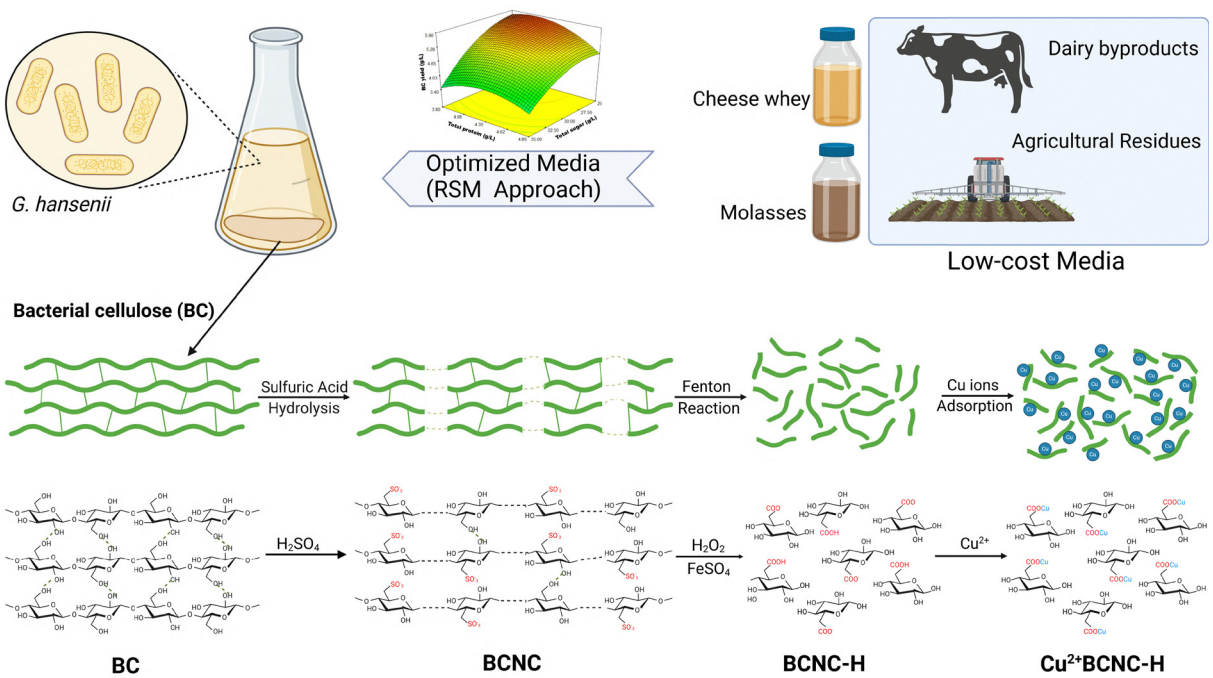

Fig. 1 The schematic diagram of BC production using a low-cost medium optimized through RSM approach, and the synthesis of carboxylated bacterial cellulose nanocrystals for Cu^{2+} ions adsorption (created with https://BioRender.com).

2. Materials and methods

2.1. Materials

BC pellicles were obtained from the static culture of *G. hansenii* (ATCC 23769, American Type Culture Collection, Manassas, VA, USA), as previously described.[23] The working culture was stored at 4 °C in Hestrin–Schramm (HS) agar medium and sub-cultured biweekly. The stock culture was maintained in 20% (v/v) glycerol at −80 °C. Sugar cane molasses was purchased from Grandma's Company, and cheese whey was prepared in the lab using the following protocol: one US gallon of whole milk (3.8 L) was heated to 95 °C for 20 min. Then, 25 mL of apple vinegar was added to induce separation of the cheese curds from the greenish liquid (cheese whey). Cupric sulfate anhydrous ($CuSO_4$) and ferrous sulfate ($FeSO_4{\cdot}7H_2O$) were purchased from Sigma, US.

2.2. BC production and growth conditions

2.2.1. Inoculum preparation. The strain was cultivated under static conditions in Hestrin–Schramm medium containing 2% (w/v) glucose, 0.5% (w/v) yeast extract, 0.5% (w/v) peptone, 0.27% (w/v) sodium phosphate dibasic (Na_2HPO_4), and 0.115% (w/v) citric acid at 30 °C. The medium's pH was adjusted to 5.5 using 1 M HCl or NaOH, then sterilized by autoclaving at 121 °C for 20 min. The culture grew until an optical density (OD) of 0.9 at 600 nm was reached. The seed culture was then vigorously shaken to release bacteria trapped within the pellicles into the medium, and a 10% (v/v) inoculum was added to either the main culture or the control (HS medium).

2.2.2. Optimization of BC through CCD and analysis of data. A CCD method with four independent variables was used to determine optimal conditions for BC production (dried weight, g L^{-1}) using a low-cost medium composed of molasses and cheese whey. The variables included total sugar concentration (A, g L^{-1}), total protein concentration (B, g L^{-1}), acetic acid concentration (C, % (v/v)), and pH (D). Each factor was tested at five levels ($-\alpha$, −1, 0, +1, and $+\alpha$), with $\pm\alpha$ values set to ±2 based on Montgomery's guidelines.[26] Table 1 provides the parameter boundaries established from our previous study.[23] Design Expert software (version 7.1.5; Stat-Ease, Inc., USA, Windows) was used to generate the experimental design matrix and perform analysis. The model was evaluated with Fisher's statistical test for analysis of variance (ANOVA), and all three-dimensional CCD graphs were created using Design Expert software. Table S1 (SI) presents the experimental matrix, comprising 30 experiments, including 16 factorial points, 8 axial points, and 6 center points. The response variable, dried BC production (g L^{-1}), was measured under static conditions at 30 °C after 8 days of cultivation. All experiments were carried out independently in triplicate, following the sequential order outlined in Table S1. The average dried BC values are reported in Table S1.

2.3. Treatment of sugar cane molasses

Acidic hydrolysis of sugarcane molasses was conducted according to the literature.[23] In brief, a 200 mL solution of sugar cane molasses (800 g L^{-1}) was centrifuged at room temperature at 10 000 rpm for 20 min to separate and remove solid materials. The pH of the resulting supernatant was adjusted to 3.6 by adding 4 N H_2SO_4, and the mixture was left for 24 h before centrifuging again at 10 000 rpm for 20 min. The supernatant was then heated at 90 °C for 3 h to fully convert sucrose into glucose and fructose. After cooling overnight, it was centrifuged again at 10 000 rpm for 20 min, and the supernatant was neutralized using 10 M NaOH. The solution was stored for 48 h, with daily centrifugation at 10 000 rpm for 20 min to remove residual solids. The final supernatant was identified as H_2SO_4-heat-treated molasses.

2.4. Sugar analysis

2.4.1. Total sugar analysis. The phenol sulfuric acid method was used to determine the total carbohydrate content (g L^{-1}) in the culture media.[27] In summary, 1 mL of 5% w/w phenol solution was added to 1 mL of each sample in a tube. Subsequently, 5 mL of concentrated sulfuric acid (98%) was added to each tube. The tubes were shaken vigorously and allowed to cool to ambient temperature. Finally, the color intensity of the resulting solution was measured at 490 nm using a spectrometer, with D-glucose as the calibration standard.

2.4.2. Reducing sugar analysis. Reducing sugar concentration (g L^{-1}) was measured using the dinitrosalicylic acid method.[28] In brief, 3 mL of DNS reagent was added to 3 mL of each sample in a tube. The tubes were heated in a boiling water bath for 5 min, followed by the addition of 1 mL of 40% potassium sodium tartrate (Rochelle salt). To stop the reaction, the tubes were cooled to ambient temperature under running water. The color intensity of the resulting solution was then measured at 575 nm using a spectrometer, with D-glucose serving as the calibration standard.

2.5. BC purification and quantification

After 8 days of cultivation, the BC pellicles were soaked in 0.1 N NaOH solution, with the solution refreshed every 12 h over 2 days to remove the brownish color and turn the pellicles

Table 1 Variables and their levels for CCD

Variable	Unit	Symbol	Low axial ($-\alpha$)	Low factorial (−1)	Center point (0)	High factorial (+1)	High axial ($+\alpha$)
Total sugar (molasses)	g L^{-1}	A	20	25	30	35	40
Total protein (cheese whey)	g L^{-1}	B	3.25	3.8	4.35	4.89	5.44
Acetic acid	% (v/v)	C	0.15	0.25	0.35	0.45	0.55
pH	—	D	5.05	5.4	5.75	6.10	6.45

white. Then, the pellicles were treated with 0.1 N NaOH at 95 °C for 1 h to remove any bacterial biofilm, leaving only the BC matrix. The pellicles were then thoroughly washed with distilled water until reaching a neutral pH. After washing, they were carefully weighed and dried in an oven at 70 °C until a constant mass was achieved. The dried weight was used to calculate the production yield in g L^{-1} (dry weight of BC (g)/volume of the original culture media (L)). Additionally, the productivity was expressed in g L^{-1} day^{-1} (dry weight of BC/(volume of the original medium/number of cultivation days)). Furthermore, medium efficiency was calculated based on BC production (g L^{-1}) relative to total sugar consumption (g L^{-1}). For metal adsorption experiments, the purified wet pellicles were further processed with either H_2SO_4 or H_2O_2 treatment, as outlined in Section 2.6.

$$\text{BC production yield} = \frac{\text{Dried BC(g)}}{\text{Culture medium volume (l)}} \quad (1)$$

$$\text{BC productivity} = \frac{\text{Dried BC(g)}}{(\text{Culture medium volume (l)} \times \text{day})} \quad (2)$$

$$\text{Medium efficiency}\ (\%) = \frac{\text{BC production yield}\ (\text{g L}^{-1})}{\text{Total sugar consumption}\ (\text{g L}^{-1})} \times 100 \quad (3)$$

2.6. BCNCs and BCNCs-H preparation

BCNCs were prepared following previously reported methods with minor modifications.[29,30] Briefly, purified wet BC pellicles were disintegrated into a BC paste using a laboratory blender at 6000 rpm for approximately 20 minutes at 20 °C. The resulting BC paste was centrifuged at 10 000 rpm for 15 min at 20 °C to remove excess water. For BCNC synthesis, 5 g of BC paste was dispersed in 50 mL of 50% (w/w) sulfuric acid and heated at 45 °C for 1 hour under vigorous magnetic stirring. The reaction was quenched by diluting the system 5-fold with cold distilled water, followed by centrifugation at 10 000 rpm for 15 min at 20 °C to separate crystals from acid. The crystals were washed multiple times with distilled water and centrifuged at 10 000 rpm for 15 minutes at 20 °C until the pH reached approximately 4.5.

To prepare BCNCs-H, a modified version of the method proposed by Fan *et al.* was used.[15] Three grams of wet BCNC produced in the previous stage was dispersed in 33.5 mL of distilled water. Subsequently, 100 μL of fresh 0.1 M $FeSO_4{\cdot}7H_2O$ solution was added to the mixture followed by adjusting the pH to 3.5 using 1 M HCl. The mixture was heated up to 42 °C under stirrer condition (260 rpm). After reaching the temperature of 42 °C, 16.5 mL of 30% (w/w) H_2O_2 was added dropwise to the mixture in 1 hour. The reaction continued for more 1.5 hours (2.5 hours from adding the first drop of H_2O_2) to convert BCNCs to BCNCs-H. Next, the mixture was centrifuged at 10 000 rpm for 15 min at 20 °C to remove excess H_2O_2 from the crystals. The crystals were washed and centrifuged three times. Finally, the resulting BCNCs-H suspension was dialyzed against distilled water using a dialysis membrane with a molecular weight cutoff of 3500 Da to neutralize the suspension and remove low-molecular-weight impurities. The dialysis water was replaced every 12 hours to ensure effective purification. Finally, the purified BC without treatment, BCNCs or BCNCs-H were freeze-dried at 0.01 bar and −50 °C. The freeze-dried crystals were ground using a laboratory mortar and pestle. The prepared samples were used for subsequent copper adsorption studies, as well as SEM, FT-IR, XRD, XPS, and thermal gravimetric analysis.

2.7. Characterization of BC, BCNC, and BCNCs-H

To investigate the impact of sulfuric acid treatment and the oxidation process on the morphology, surface characteristics, and structure, each sample was analyzed using SEM, FTIR, XRD, zeta potential, and TGA. BC, BCNC, and BCNC-H refer to pure bacterial cellulose without treatment, BC after sulfuric acid treatment, and BCNC after oxidation *via* the Fenton reaction, respectively. BCNC-H and BC (control) were used to study the effect of –COOH groups on copper ion adsorption. Additionally, XPS analysis was performed on BC and BCNC-H (before and after adsorption) to examine surface coverage and binding mechanisms.

2.7.1. Morphology characterization. To study the morphology of the samples, freeze dried BC, BCNC, and BCNC-H were observed using a JEOL JSM-6700F field emission scanning electron microscope (FE-SEM) operating at 5 kV. Scale bars were added using ImageJ software, developed by the U.S. National Institutes of Health in Bethesda, Maryland, USA. Fiber width measurements were conducted using image J software across 200 random points for each sample.

2.7.2. FTIR spectroscopy. FTIR measurements were recorded through a Thermo Fisher Nicolet iS50 FTIR in the range of 400–4000 cm^{-1} with a resolution of 16 cm^{-1} for 32 scans at ambient temperature.

2.7.3. XRD. XRD profiles of BC, BCNC, and BCNC-H were collected at room temperature in the 2θ range of 5°–30° with a step size of 0.05° and scan speed of 2° min^{-1} using a Rigaku SmartLab equipment with Cu-Kα radiation (λ = 0.154 nm) generated at 40 kV and 40 mA. SmartLab Studio II (version 4.6.426.0) software was used to analyze the diffraction diagrams. The sample crystallinity index (CrI) % was calculated using the Segal method[31] with the following equation:

$$\text{CrI}\% = \left(\frac{I_{110} - I_{\text{am}}}{I_{110}}\right) \times 100 \quad (4)$$

where I_{110} and I_{am} are the peak intensity of [110] at 2θ = 22.7°, and [010] at 2θ = 18°, respectively.

The crystallite sizes (CrS) (nm) were calculated using Scherrer's equation[32] as shown in eqn (5):

$$\text{CrS} = \frac{K\lambda}{\beta \cos\theta} \quad (5)$$

K is the shape factor, which depends on the method used to determine the peak breadth (K = 0.94 in this study). λ represents the wavelength of the incident X-ray (λ = 0.154 nm),

β is the full width at half maximum intensity (FWHM) in radians, and θ is the peak center angle.

2.7.4. XPS. XPS spectra were recorded using an ESCALAB Xi spectrometer (Thermo Fisher Scientific) equipped with monochromatized Al Kα radiation ($h\nu$ = 1486.7 eV), with the anode operated at 225 W and 30 kV. All spectra were calibrated using the C 1s peak at 284.8 eV. Data deconvolution was performed using Thermo Avantage software. The instrument operated at a working pressure of 6×10^{-7} mbar.

2.7.5. Zeta potential. The zeta potential of the samples at different pH levels (3–9) was measured using a Malvern Zetasizer ultra (UK) at 25 °C. For each measurement, 3 mg of wet samples (BC, BCNC, and BCNC-H) were dispersed in 10 mL of distilled water. The pH was adjusted using 0.1 M HCl or 0.1 M NaOH. The dispersions were sonicated in a water bath for 1 hour, followed by vortexing for 5 minutes before analysis. To obtain 3 mg of wet samples (BC, BCNC, and BCNC-H), each suspension was centrifuged at 10 000 rpm for 15 minutes at 20 °C to remove the water. The separated samples were then centrifuged again under the same conditions to eliminate excess water and prepare them for weighing. The reported zeta potential values represent the average of five measurements, with each measurement conducted in triplicate.

2.7.6. Thermal gravimetric analysis. Thermal gravimetric analysis (TGA) and the derivative of thermogravimetric (DTG) of BC, BCNC, and BCNC-H were studied using a TGA instrument (TGA 5500, USA). Approximately, 10 mg of each sample was heated up in the range of 20 °C to 600 °C using a 100 mm platinum pan. The nitrogen gas flow rate and the heating rate were set to 25 mL min^{-1} and 10 °C min^{-1}, respectively. The weight loss (%) and the first derivative of the weight loss (%) were plotted against the temperature.

2.8. Adsorption experiments

Adsorption experiments were conducted through a batch-wise technique. All the experiments were carried out using a shaker at 100 rpm under an ambient temperature (25 °C). To study the impact of carboxyl groups on copper adsorption, 2.5, 5, and 10 mg of each adsorbent (BC and BCNC-H) was added to 20 mL of a 50 mg L^{-1} copper solution at pH 5. The mixtures were placed in 125 mL flasks and stirred for 3 hours to ensure equilibrium was reached. The adsorption efficiency (%) and uptake capacity of the adsorbents (mg g^{-1}) after 3 hours were calculated using eqn (6) and (7).

$$S\,(\%) = \left(\frac{C_0 - C_t}{C_0}\right) \times 100 \tag{6}$$

$$q_t = \left(\frac{C_0 - C_t}{m}\right) \times V \tag{7}$$

where C_0, C_t, m, and V represent the initial concentration of copper in the solution (mg L^{-1}), the copper concentration after 3 hours (mg L^{-1}), the absolute dry mass of the adsorbent (g), and the volume of the copper solution (L), respectively. All experiments were performed in triplicate, and the results are presented as the mean ± standard deviation (SD). Copper ion concentrations in the solution were measured using an Agilent 7900 ICP-MS.

3. Results and discussions

3.1. Optimization of BC through CCD and analysis of data

RSM through a CCD approach was applied to investigate individual and interactive effects of the studied parameters including total sugar and total protein concentration (g L^{-1}), acetic acid concentration % (v/v), and the initial pH of the culture media. According to the results shown in Table S1 the highest yield (g L^{-1}) is associated with experiment 19, where total sugar, total protein, acetic acid, and pH set at 25 (g L^{-1}), 3.8 (g L^{-1}), 0.45% (v/v), and 6.1; under these conditions, the average BC production was 6.17 ± 0.19 (g L^{-1}), and 93% (23.25 g L^{-1}) of initial total sugar were consumed after 8 days of the cultivation. This represents a 6.85-fold increase compared to the BC production of control samples using HS medium which resulted in the production of 0.9 ± 0.08 g L^{-1} of BC. Based on material costs, the molasses–cheese whey medium used in this study reduced the production cost of 1 g of dried BC to 0.105 USD, representing an approximately 65-fold decrease compared to the synthetic HS medium (6.915 USD). Based on the ANOVA analysis of the experiments shown in Table 2, a quadratic model was proposed to explain the relation between the response (BC yield (g L^{-1})) and the studied factors. The statistical significance of the model with an F-test of 20.83 and p-value <0.0001 confirms that the model is significant. Additionally, the lack of fit, p = 0.2391, is not significant, indicating that there is just a 23.91% chance that a ''lack of fit F-value'' this large could occur due to noise. The second-order polynomial equation describing the relationship between the response and the studied factors (based on actual factors) is:

$$\begin{aligned} Y = {} & -82.91 + 0.8A + 15.08B + 20.9C + 14.65D \\ & + 0.093AB - 0.44AC - 0.014AD - 1.41BC \\ & - 0.605BD - 0.55CD - 0.019A^2 - 1.64B^2 \\ & - 0.366C^2 - 0.95D^2 \end{aligned} \tag{8}$$

where Y, A, B, C, and D were BC yield (g L^{-1}), total sugar (g L^{-1}), total protein (g L^{-1}), acetic acid concentration % (v/v), and the initial pH of the medium, respectively. The coefficient of determination (R^2) indicates the extent to which the variability in the observed response values can be explained by the model. An R^2 value of 0.9511 indicates that over 95% of the response variation can be explained by the proposed model. Fig. S1 shows the actual values *versus* the predicted values for each experiment using eqn (8). The adjusted R^2, which considers the sample size and number of variables, is also satisfactory at 0.9054 and is close to the R^2 value.

The optimization function of the Design Expert software was used to identify the optimal conditions for BC production based on the investigated factors. To maximize the yield the software set total sugar (g L^{-1}), total protein (g L^{-1}), acetic acid % (v/v), and the initial pH of the medium to 21.76, 3.84, 0.55,

Table 2 ANOVA analysis of CCD experiments and quadratic model

Source	Sum of squares	D_f	Mean square	F-Value	p-Value	
Model	33.89	14	2.42	20.83	<0.0001	Significant
A-molasses	17.70	1	17.70	152.29	<0.0001	Significant
B-cheese whey	0.99	1	0.99	8.54	0.0105	Significant
C-acetic acid	0.90	1	0.90	7.79	0.0137	Significant
D-pH	0.59	1	0.59	5.13	0.0387	Significant
AB	1.03	1	1.03	8.90	0.0093	Significant
AC	0.78	1	0.78	6.74	0.0202	Significant
AD	0.01	1	0.01	0.093	0.7635	Not significant
BC	0.09	1	0.094	0.81	0.3806	Not significant
BD	0.21	1	0.21	1.83	0.1955	Not significant
CD	0.005	1	0.005	0.05	0.8244	Not significant
A^2	6.23	1	6.23	53.60	<0.0001	Significant
B^2	6.52	1	6.52	56.10	<0.0001	Significant
C^2	0.0003	1	0.0003	0.003	0.9558	Significant
D^2	0.37	1	0.37	3.19	0.0940	Not significant
Residual	1.743923	15	0.11			Not significant
Lack of fit	1.38	10	0.13	1.94	0.2391	Not significant
Pure error	0.35	5	0.071			
Cor total	35.64309	29				
R^2	0.9511					
Adj R^2	0.9054					
Pred R^2	0.7613					
Adeq precision	17.59					

and 6.15, respectively. The predicted BC production under these optimal conditions was 6.25 (g L^{-1}). To validate the prediction, experiments were conducted in triplicate at the suggested optimal point and the observed BC production was 6.13 ± 0.17 g L^{-1}, which was not significantly different from the predicted value ($p > 0.05$). In our previous study,[23] OFAT method was employed to study the impact of total sugar in molasses (g L^{-1}), total protein in cheese whey (g L^{-1}), acetic acid concentration % (v/v), and initial pH on BC production. Using the OFAT method resulted in BC production of 5.11 g L^{-1} in a medium containing 30 g L^{-1} total sugar, 4.34 g L^{-1} total protein, 0.4% (v/v) acetic acid, and an initial pH of 6. However, applying a CCD approach led to a higher BC yield of 6.17 g L^{-1}, a 20.7% increase in production. Furthermore, the medium efficiencies for the CCD and OFAT methods were 26% and 19.57%, respectively. These findings demonstrate that utilizing CCD instead of traditional methods improves efficiency, saving both time and cost. Rodrigues *et al.*[33] used the CCD method for BC production and reported a yield of 7.5 ± 0.54 g L^{-1} after nine days of cultivation. This yield was obtained with total sugar consumption of 46.8 g L^{-1} and a media efficiency of 16.02%, which was remarkably lower than that observed in this study. Although they, like in this study, used molasses as a carbon source, they did not hydrolyze it. As a result, their media contained sucrose, glucose, and fructose. In contrast, in this study, molasses was hydrolyzed, thereby converting the disaccharide sucrose into the monosaccharides, glucose and fructose, which are more favorable for biological processes and BC production. Table 3 compares the BC productivity (g L^{-1} day^{-1}) obtained in this research with values reported in other studies using low-cost substrates under static conditions, indicating that the present work demonstrates a promising strategy for economical BC production. 3D surface graphs (Fig. 2) illustrate the interactions between two factors at a time in relation to BC yield (g L^{-1}), while the other factors remain at their zero levels. Higher total sugar concentrations (30–40 g L^{-1}), regardless of total protein concentration, were not suitable for BC production (Fig. 2a). This may be attributed to the formation of gluconic acid, a byproduct in the BC synthesis pathway, that typically occurs in media with excess carbon sources.[23,34] However, lower total sugar concentrations, particularly when total protein concentration was below 4.35 g L^{-1}, resulted in higher BC yields. The carbon-to-nitrogen (C/N) ratio plays a crucial role in biological processes such as BC production. Thus, even at lower total sugar concentrations, higher protein concentrations were not conducive to BC production. In this study, the highest BC yield (6.17 g L^{-1}) was observed in experiment 19, where the C/N ratio was 6.57. A previous study[23] using the OFAT approach reported the highest BC yield at a C/N ratio of 6.9. Additionally, Zhang *et al.*[35] studied the effect of C/N ratios on BC synthesis using *Acetobacter xylinum* NUST4.2 and found that while a C/N ratio of 5.39 favored cell growth, a ratio of 6.31 was optimal for BC production. Fig. 2b depicts the interaction between total sugar concentration (g L^{-1}) and acetic acid concentration (% v/v) and their influence on BC yield. The data shows that adding acetic acid to media with lower total sugar concentrations significantly enhanced BC production. This might be due to the role of acetic acid in the tricarboxylic acid (TCA) cycle, where it enters as an intermediate component, thereby boosting ATP production.[36] Additionally, acetic acid can increase glucose availability for BC synthesis by participating in the gluconeogenesis pathway.[37] However, at higher total sugar concentrations, acetic acid supplementation reduced BC production. This may be due to the excess carbon source in the medium, which inhibits bacterial growth, increases gluconic acid production, and subsequently lowers the pH. Fig. 2c highlights the interaction between pH and total sugar concentration on BC production,

Table 3 Bacterial cellulose production using low-cost medium under static conditions in different studies

Bacteria name	Carbon source (g L^{-1})	Nitrogen source	Additives	Culture volume (mL) & flask scale (mL)	Productivity (g L^{-1} day^{-1})	Ref.
G. hansenii ATCC 23769	Molasses (25 g L^{-1})	Cheese whey	Acetic acid	25 & 125	0.77	This study
G. hansenii ATCC 23769	Molasses (30 g L^{-1})	Cheese whey	Acetic acid	25 & 125	0.64	23
Komagataeibacter europaeus BCRC 14148	Pineapple core hydrolysate (30 g L^{-1})	Peptone, yeast extract	Buffer	3 & glass tubes	0.72	38
Komagataeibacter xylinus BRP 2001 (ATCC 700178)	Molasses (53.8 g L^{-1})	Corn steep liquor	Ethanol, ammonium sulphate, buffer	40 & 100	0.83	33
Komagataeibacter hansenii ATCC 23769	Sisal juice (15 g L^{-1})	Yeast extract	—	100 & Petri dishes	0.338	39
Gluconacetobacter kombuchae (MTCC NO. 6913)	Enzymatically hydrolyzed rice straw (14.67 g L^{-1})	Yeast extract, peptone	Buffer	Not mentioned	0.51	40
Lactiplantibacillus plantarum strain AS.6	Enzymatically hydrolyzed prickly pear peels (PPP) (12.09 g L^{-1})	—	—	Not mentioned	0.546	41
Komagatacibacter xylinus PTCC1734	Molasses (20 g L^{-1})	—	—	150 & 300	0.32	22
	Enzymatically hydrolyzed cheese whey (30 g L^{-1})	—	—		0.25	
Gluconacetobacter xylinus ATCC 53582	Cashew apple juice (20 g L^{-1})	Soybean molasses	—	50 & 250	0.64	42

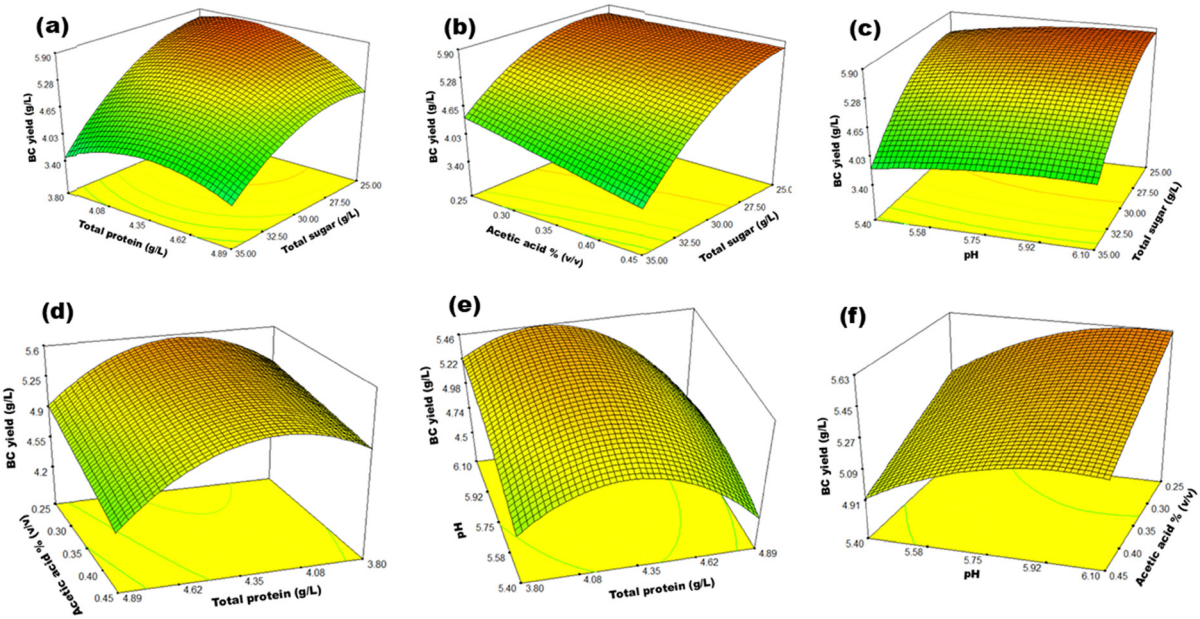

Fig. 2 Response surface curves of BC production: (a) total sugar (g L^{-1}) and total protein (g L^{-1}); (b) total sugar (g L^{-1}) and acetic acid % (v/v); (c) total sugar (g L^{-1}) and pH; (d) total protein (g L^{-1}) and acetic acid % (v/v); (e) total protein and pH; (f) acetic acid % (v/v) and pH.

which was most pronounced at lower total sugar concentrations. As pH increased, its effect on BC yield became more significant. Fig. 2d and e illustrate the effects of total protein and acetic acid concentrations, as well as total protein concentration and pH, on BC production, respectively. The BC yield increased at lower acetic acid concentrations and higher pH levels. Similarly, Fig. 2f depicts the interaction between pH and acetic acid concentration, showing that BC yield was higher at lower acetic acid concentrations and elevated pH levels.

3.2. BCNC-H synthesis

Cellulose is a polysaccharide with a relatively low negative charge due to the presence of hydroxyl groups (pK_a value of hydroxyl groups, ~12–13.5[43]), making it less effective at chelation of charged moieties, specially at lower pH. Previous work demonstrates that BC interacts with water and its solutes, enabling one-step hybrid material synthesis and metal binding.[44] Modification of BC to include carboxyl groups (–COOH) enhances these interactions due to the inclusion of a negative charge to the polymer. To functionalize BC, we used a Fenton reaction mechanism consisting of an oxidizing agent (H_2O_2) and a catalyst ($FeSO_4{\cdot}7H_2O$) to synthesize BCNC-H from wet BCNC. In the presence of a catalyst such as Fe^{2+}, H_2O_2 dissociates into protons (H^+), hydroxyl radicals ($OH^\bullet$), and H_2O_2. These highly active $OH^\bullet$ radicals attack the –OH groups on the BCNC surface, leading to the carboxylation of BCNC

(BCNC-H). Additionally, under acidic conditions, H^+ ions can protonate β (1 → 4) glycosidic bonds, resulting in the cleavage of these linkages and modification of the BC structure. Since adding H_2O_2 lowers the system's pH, the initial pH was set to 3.5 to prevent excessive acidification and unwanted degradation or hydrolysis of BC. In this study, we observed a decrease in pH from 3.5 to 2.7. The mechanisms of the Fenton reaction are illustrated in the following equations:[45]

$$Fe^{2+} + H_2O_2 \rightarrow Fe^{3+} + OH^{\bullet} + OH^{-} \quad (9)$$

$$Fe^{3+} + H_2O_2 \rightarrow Fe^{2+} + OOH^{\bullet} + H^{+} \quad (10)$$

$$OH^{\bullet} + OH^{\bullet} \rightarrow H_2O_2 \quad (11)$$

$$RCH_2OH + OH^{\bullet} \rightarrow R^{\bullet}CHOH + H_2O \quad (12)$$

$$R^{\bullet}CHOH + H_2O_2 \rightarrow RCHO + OH^{\bullet} + H_2O \quad (13)$$

$$RCHO + 2OH^{\bullet} \rightarrow RCOOH + H_2O \quad (14)$$

In this study, multiple attempts were made to directly carboxylate BC, rather than BCNC, using the Fenton reaction. However, the results were weak or inconsistent in confirming the formation of –COOH groups on the BC surface. Chang and Chen[46] reported weak carboxylation of wet BC using only H_2O_2, without the Fenton reaction, however we found that effective carboxylation occurs only when BCNC is subjected to the Fenton reaction. This may be attributed to the increased surface area of BCNC compared to BC, allowing a higher percentage of the materials to be exposed to highly active $OH^{\bullet}$ radicals. Additionally, the dispersion of BCNC in distilled water significantly improved due to the presence of sulfate groups, which enhanced electrostatic repulsion. In contrast, BC exhibited strong aggregation around the magnetic stirrer, reducing the efficiency of the Fenton reaction. Furthermore, the duration, temperature, and concentration of H_2SO_4 play a crucial role in the acidic treatment of BC. Prolonged exposure and higher temperatures significantly intensified the reaction between BC and acid, leading to substantial structural changes in BCNC.[11] Consequently, the subsequent Fenton reaction between BCNC and H_2O_2 becomes more aggressive, resulting in increased material loss. In this study, the yield of BCNC-H obtained from BC was 66%. In another study, Yan *et al.*[29] reported the production of BCNC by treating 5 g of wet BC using 80 mL of 50% (w/w) sulfuric acid for 3 hours at 45 °C, followed by carboxylation of BCNC through the addition of 8 mL of 30% H_2O_2 and subsequent centrifugation (no heating was mentioned). In this study, the material cost for producing 1 g of dried BCNC-H using the low-cost medium was 30.6 USD, which could be further reduced through large-scale production.

3.3. Characterization of BC, BCNC, and BCNC-H and adsorption experiments

3.3.1. Morphology of BC, BCNC, and BCNC-H. SEM images illustrate substantial changes in the morphology of BC samples after H_2SO_4 treatment and the Fenton reaction (Fig. 3(a)–(c)). Although BCNC and BCNC-H exhibit an entangled and intertwined structure similar to BC, there is a significant difference in the fiber width of the samples (Fig. 3(d)–(f)). While the fiber width of BC ranges from 40 to 180 nm, BCNC fibers vary between 20 and 110 nm. This reduction is attributed to the hydrolysis of glycosidic bonds due to the H_2SO_4 treatment of BC.[11,29] BCNC-H displays finer fibrils compared to both BC and BCNC, with fiber diameters ranging from 10 to 37 nm which is consistent with the literature.[15,47] The average fiber diameter of BC, BCNC, and BCNC-H was 90.94 ± 24.35 nm, 63.45 ± 14.86 nm, and 24.43 ± 5.6 nm, respectively. The high standard

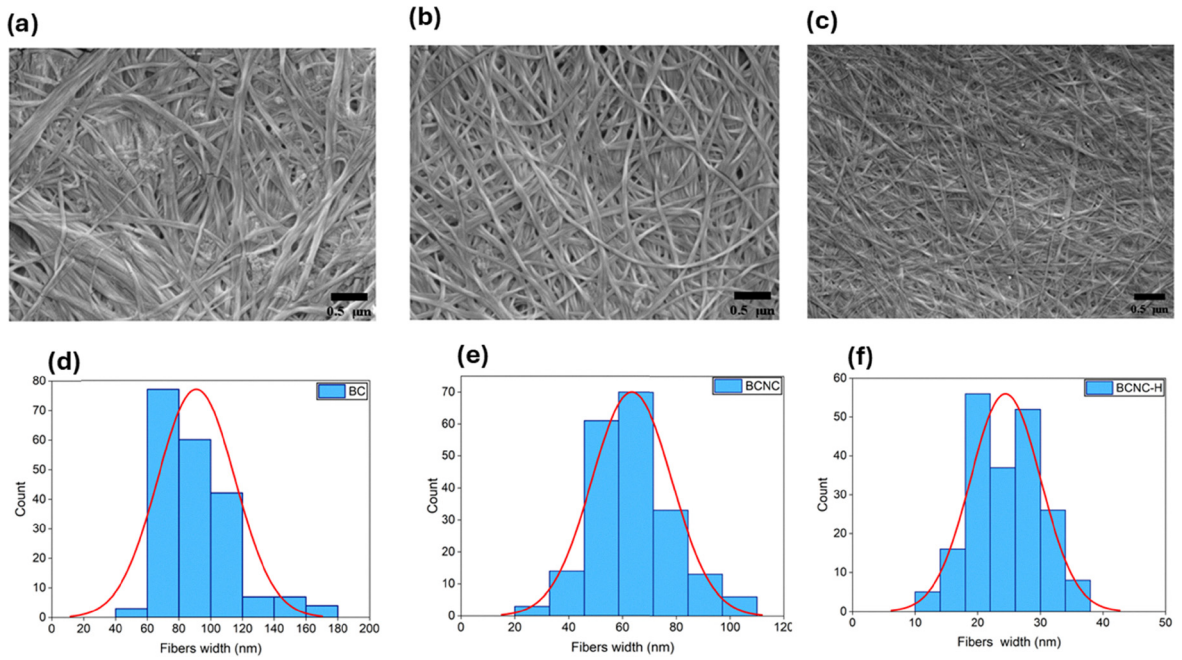

Fig. 3 SEM images of BC (a), BCNC (b), and BCNC-H (c). The Fiber width and normal distribution of BC (d), BCNC (e), and BCNC-H (f).

deviation of BC is due to the broad range of fiber widths in the sample. Jafari *et al.*,[23] Jacek *et al.*,[48] and El-Gendi *et al.*[41] reported fiber widths of BC in the ranges of 35–188 nm, 60–160 nm, and 0–400 nm, respectively.

3.3.2. FTIR. FTIR analysis was used to identify the functional groups and structural changes on the surfaces of both unmodified and modified BC samples. No significant differences were observed between the FTIR spectra of BC, BCNC, and BCNC-H, except for a newly emerged peak at 1734 cm^{-1}, attributed to –COOH groups in BCNC-H.[49] Due to the high oxidative capability of H_2O_2, the –OH groups at the C-6 position in glucose were oxidized to –COOH groups (Fig. 4a).[46] The peak at 3340 cm^{-1} corresponds to the stretching vibration of –OH groups.[50] The hydroxyl stretching peak appears sharper in BCNC-H compared to BC and BCNC, indicating that the Fenton reaction may have disrupted intramolecular hydrogen bonding in BC and BCNC, leading to the cleavage of glycosidic bonds (Fig. 4a).[51] Additionally, the peak around 2900 cm^{-1} corresponds to C–H stretching in CH_2 and CH_3 groups, while the peak at 1640 cm^{-1} is assigned to the bending vibration of –OH groups of absorbed water. Moreover, no peak was detected at the 807 cm^{-1} band in BCNC and BCNC-H, which corresponds to the symmetric vibration of the C–S bond in C–O–SO_3^- groups. This absence is likely due to the small amount of sulfate groups on the surface, making them undetectable by FTIR. Notably, Singhsa *et al.*,[12] Pinto *et al.*,[52] and Arserim-Uçar *et al.*,[11] in FTIR separate studies, also failed to detect the 807 cm^{-1} peak for C–O–SO_3^- groups, despite using higher temperatures, longer reaction times, and greater acid concentrations than those used in this study. However, as discussed in Section 3.3.4., zeta potential data may provide further evidence of sulfate groups on the BCNC surface.

3.3.3. XRD. XRD analysis was performed to assess the crystalline structure of the synthesized BC materials. The characteristic peaks of cellulose Iα,[23] approximately 14.5° ([100]), 16.8° ([010]), and 22.7° [110] were observed in all samples, confirming that the bacterial cellulose crystalline form was retained after sulfuric acid treatment and Fenton oxidation. A slight increase in CrI (%) and crystallite size was observed for BCNC compared to BC, likely due to the removal of amorphous regions following acidic treatment.[11,12] BCNC-H showed a minor decrease which may be attributed to the breakdown of the glucopyranose ring or the cleavage of glycosidic bonds during oxidation, leading to a more disordered cellulose structure.[30,53] Detailed diffraction patterns and crystallite size data are provided in the SI (Fig. S2 and Table S2).

3.3.4. Zeta potential of BC, BCNC, and BCNC-H. Surface charge and degree of ionization of adsorbents play crucial roles in metal ion adsorption.[54] Functionalized materials exhibit varying surface charges, either negative or positive, depending on the pH. BC and BCNC follow a similar trend in zeta potentials, with only slight differences in zeta potential values across pH from 3 to 9 (Fig. 4b). The more negative surface charge of BCNC compared to BC is attributed to the acidic treatment of BC with 50% (w/w) H_2SO_4, which introduces –OSO_3^- groups on its surface. However, we didn't detect any sulfate group FTIR peak at 807 cm^{-1} on the BCNC surface, which is possibly due to the small amount. The absolute zeta potential of BCNC-H is significantly higher than that of BC and BCNC (Fig. 4b). We attribute the strong negative charge of the functionalized BC to the presence of –COOH groups on the BCNC-H surface, introduced *via* oxidation of BCNC using the Fenton reaction. At acidic pH values (below the pK_a value of carboxyl groups, ~3–4[55]), most carboxyl groups remain protonated due to the higher concentration of H^+ ions, resulting in a lower surface charge. As the pH increases, the H^+ concentration decreases, leading to the ionization of carboxyl groups (–COOH → –COO^-). Consequently, at higher pH values, the negative surface charge of BCNC-H increases, enhancing its

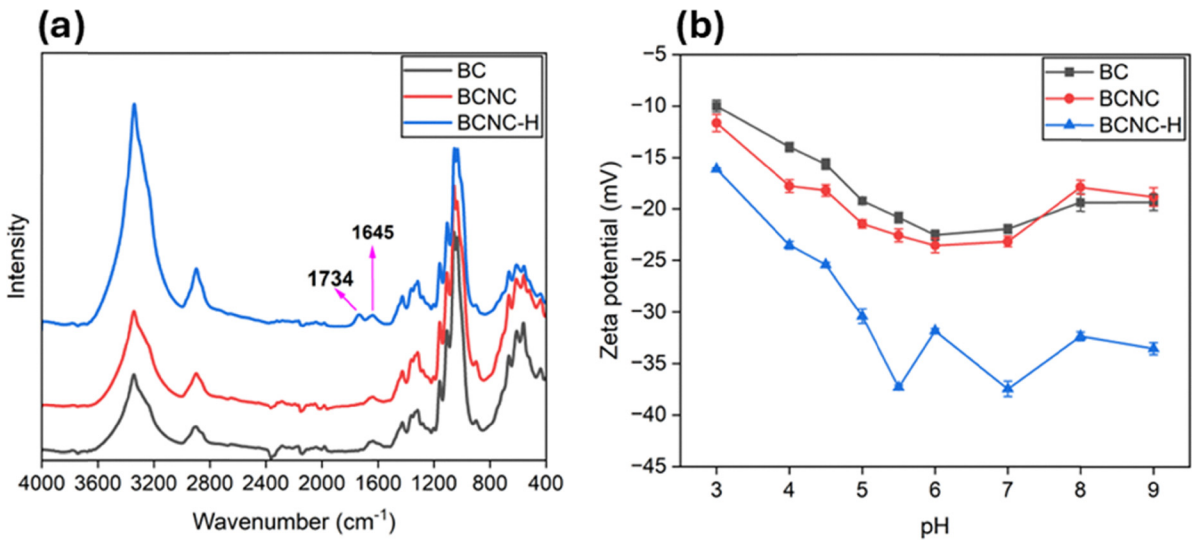

Fig. 4 (a) FTIR spectra and (b) zeta potential of BC (black), BCNC (red), and BCNC-H (blue). The emergence of the peak at 1734 cm^{-1} (FTIR) indicates the addition of –COOH groups on BCNC-H.

electrostatic interactions. The negative surface charge of BCNC-H is in good agreement with the previous research.[15,56]

3.3.5. Thermal gravimetric analysis. The thermal behaviors of BC, BCNC, and BCNC-H were analyzed using TGA and DTG to evaluate the effects of sulfuric acid treatment and oxidation on the thermal stability of the BC samples. Each sample demonstrated three stages of weight loss (Fig. 5a). The first stage, occurring between 25 °C and 100 °C, corresponds to the dehydration of adsorbed water, with no significant differences among the samples (Fig. 5a). The second stage, which accounts for the primary weight loss, varies significantly between samples. This degradation is attributed to the decomposition of glucose units, dehydration, and depolymerization, followed by the formation of char residues.[23] The weight loss during the second stage was 79%, 74%, and 64% for BC, BCNC, and BCNC-H, respectively. The DTG curve (Fig. 5b) illustrates variations in the onset degradation temperature (T_0) and maximum decomposition temperature (T_{max}). As shown in Table 4, T_0 and T_{max} for BC are significantly higher than those for BCNC and BCNC-H. The lower thermal stability of BCNC when compared to BC may be attributed to the presence of sulfate groups on its surface, which can catalyze dehydration by reducing the activation energy and increasing the thermal degradation rate.[11,12,57] Additionally, the presence of thermally unstable –COOH groups on the surface of BCNC-H further reduced its thermal stability compared to BCNC. This decrease may be attributed to the disruption of hydrogen bonding within the cellulose structure during the formation of carboxyl groups. Furthermore, SEM images (Fig. 3) show that sulfuric acid treatment and the Fenton reaction produced fibers with smaller sizes and a larger specific surface area compared to BC, leading to lower thermal stability. These results are consistent with the previous research.[15] Nevertheless, despite the decrease in thermal stability of BCNC-H relative to BC, it still demonstrates sufficient thermal resistance for use in various industrial applications.

Table 4 Thermal parameters of the BC, BCNC, and BCNC-H

Sample	T_0 (°C)	T_{max} (°C)
BC	306	358
BCNC	249	328
BCNC-H	244	316

3.3.6. Copper ions adsorption. A series of batch experiments were conducted to evaluate the impact of –COOH groups on Cu^{2+} adsorption. A higher negative surface charge enhances the chelation with cationic ions. Zeta potential data (Fig. 4b) revealed that BCNC-H exhibits a higher absolute negative surface charge at pH 5.5 (−37.3 mV) and pH 7 (−37.46 mV) compared to the other studied pH values. However, due to the very low solubility product constant (K_{sp} = 2.2 × 10^{-20}) of $Cu(OH)_2$,[58] a pH less than 5.8 is required to dissolve 50 mg L^{-1} of copper ions, above which it begins to precipitate. To prevent precipitation and ensure more accurate adsorption measurements, the experiments were conducted at pH 5, where the zeta potential of BC and BCNC-H were −19.2 mV and −30.4 mV, respectively. For both adsorbents (BC and BCNC-H), a lower dose (2.5 mg) resulted in a higher adsorption capacity compared to higher doses (5 and 10 mg). This may be due to the increase in unsaturation active surface sites at higher doses. It is worth noting that the optimal adsorbent dosage may vary with different concentrations of the copper ions in the solution. The adsorption capacity of BC at a 2.5 mg dosage reached 60.04 ± 6.23 mg g^{-1}, whereas BCNC-H exhibited a capacity of 164.17 ± 8.07 mg g^{-1} under the same conditions, a 173% increase (Fig. 6a). While the highest adsorption efficiency for BC was observed at a 10 mg dosage (22.86%), no significant difference was observed in the adsorption efficiency of BCNC-H across different dosages (Fig. 6b). This may be due to the increase in unsaturation active surface sites at higher doses. The other possible reason could be particle interactions, such as aggregation, which reduces the total available surface area

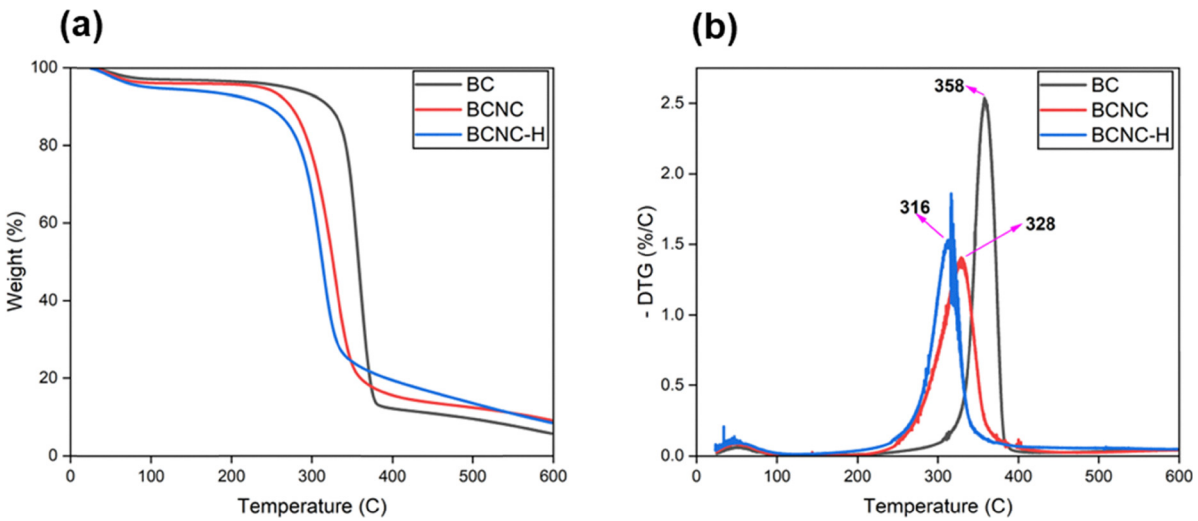

Fig. 5 TGA curves (a) and DTG curves (b) of BC, BCNC, and BCNC-H.

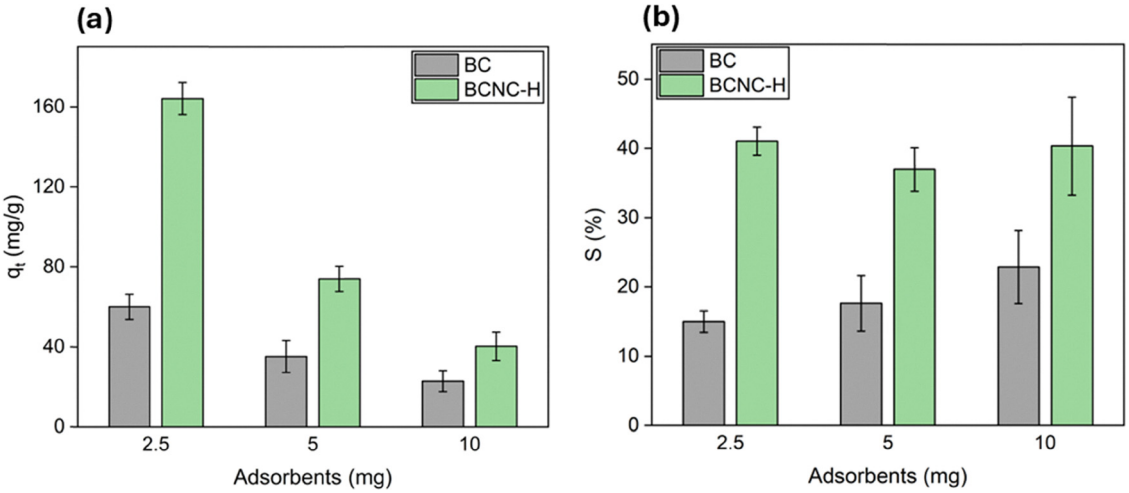

Fig. 6 (a) Adsorption capacity (mg g^{-1}) and (b) adsorption efficiency (%) of BC and BCNC-H for the removal of copper ions.

Table 5 Comparison of copper ion adsorption using different bio adsorbents

Nano/micro cellulose adsorbents	Adsorption capacity (mg g^{-1})	Ref.
BC, carboxylated BCNC	60.04, 164.17	This study
Diethylenetriamine BC	63	62
BC, BC-PHB	14.43, 37.86	63
BC, carboxymethylated BC	9.67, 12.63	59
BC, polyethyleneimine BC	79, 148	13
Carboxylated cellulose nanocrystals	51.1	15
Tempo-oxidized cellulose	75	47
Nanocellulose modified with phosphorylation	117	64
Nanocellulose modified with enzymatic phosphorylation	114	
Chemically modified rambutan peel, chemically modified passion fruit peel	192.31, 121.95	65
Alkali-modified watermelon rind	289.85	66

and increases the diffusion path length.[59–61] Table 5 compares the copper ion adsorption capacities reported in this study with those from other studies using bacterial cellulose, cellulose, or other bio-adsorbent materials. The data demonstrate that both the unmodified and carboxylated BC produced in this work shows strong potential as sustainable adsorbents for heavy metal removal. Although fewer studies have explored bacterial cellulose-based adsorbents compared to plant-derived cellulose. The findings of this study suggest that, with increased production efficiency and appropriate functionalization, bacterial cellulose-based materials could become promising alternatives for heavy metal adsorption applications. Nevertheless, certain limitations should be acknowledged. The adsorption efficiency is sensitive to solution pH and may decrease in the presence of competing ions or organic matter, which are typical components of real wastewater. In addition, the adsorbent has a finite adsorption capacity, and its performance can decline after multiple regeneration cycles. Consequently, further research using complex industrial wastewater is required to fully assess its practical applicability.

3.3.7. XPS analysis (adsorption mechanism). XPS analysis was performed to further investigate the chemical changes and surface functional groups of the adsorbents (BC and BCNC-H). The survey spectra (Fig. 7a) for both BC and BCNC-H, before and after copper ions adsorption, exhibit characteristic peaks corresponding to C 1s and O 1s. After copper ions adsorption, two distinct peaks at approximately 932 and 952 eV were observed for BCNC-H, indicating the presence of copper. In contrast, BC displayed only a very weak peak at 932 eV, suggesting limited copper binding. This weak signal in BC may be attributed to its lower adsorption capacity compared to BCNC-H. Moreover, since XPS primarily analyzes the top 3–6 nm of the surface,[67] the weaker copper signal in BC could be due to the penetration of copper ions deeper into its matrix. As seen in the SEM images (Fig. 3), BC exhibits higher porosity and thicker fibers than BCNC-H, potentially allowing deeper diffusion of copper ions and thus reducing their surface detectability by XPS. The deconvolution of the high-resolution C 1s spectrum for BC (Fig. 7b) revealed three peaks at 284.8 eV (C–C, C–H; 33.22%), 286.1 eV (C–O; 39.97%), and 287.2 eV (O–C–O, C═O; 26.81%). In contrast, the C 1s spectrum of BCNC-H (Fig. 7c) displayed an additional peak at 288.1 eV, corresponding to O–C═O groups (–COOH), indicating the successful introduction of carboxyl groups after the Fenton reaction.[68] The peak contributions for BCNC-H were 23.43% (C–C, C–H), 28.27% (C–O), 34.92% (O–C–O, C═O), and 13.37% (O–C═O). The reduction in C–O peak at 286.1 eV may be attributed to the oxidation of –OH groups into carboxyl groups.

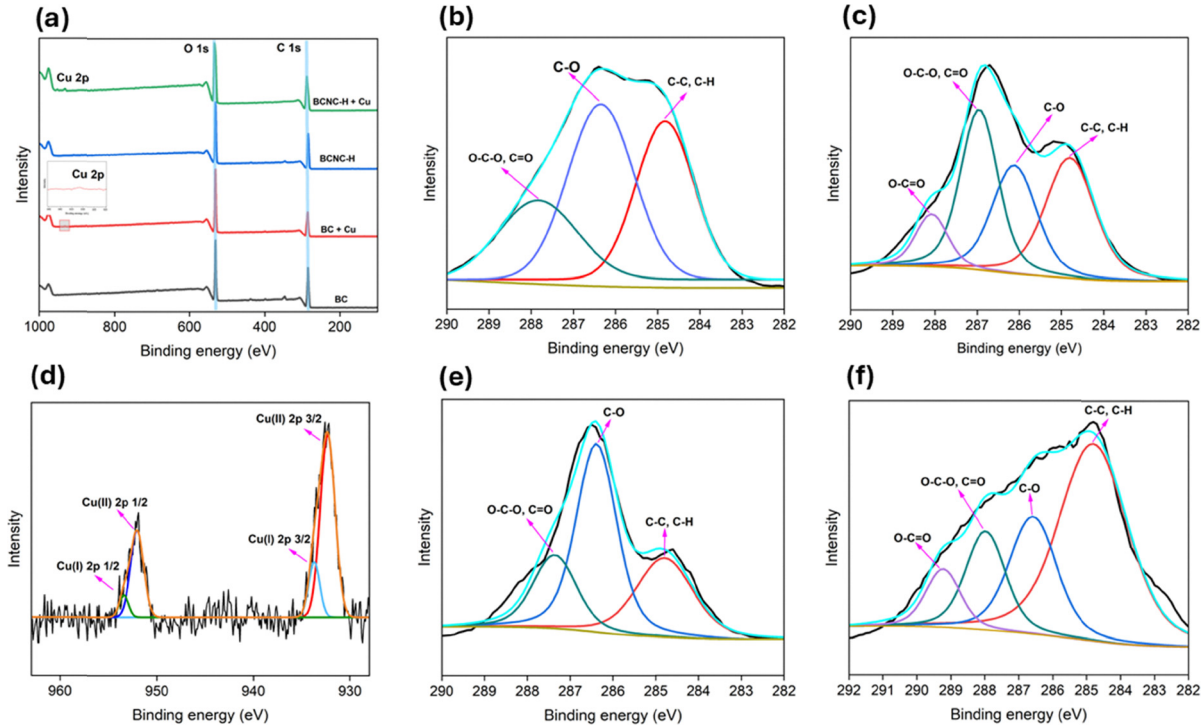

Fig. 7 (a) XPS survey of BC and BCNC-H before and after adsorption, (b) C 1s spectra of BC before adsorption, (c) C 1s spectra of BCNC-H before adsorption, (d) copper spectra of BCNC-H after adsorption, (e) C 1s spectra of BC after adsorption, (f) C 1s spectra of BCNC-H after adsorption.

Consequently, this conversion resulted in an increased intensity of the peak at 287.2 eV (O–C–O, C═O) and the appearance of a new peak at 288.1 eV. Moreover, the oxidation reaction led to the cleavage of C–C bonds in D-glucopyranose,[69] causing a decrease in the intensity of the peak at 284.8 eV compared to BC. The O/C ratios of BC and BCNC-H were 0.55 and 0.68, respectively, confirming the successful oxidation of BC. After copper ion adsorption, BCNC-H exhibited Cu 2p XPS peaks at 932.4 and 933.7 eV, corresponding to Cu(II) $2p_{3/2}$ and Cu(I) $2p_{3/2}$, respectively, while peaks at 952.1 and 953.5 eV were assigned to Cu(II) $2p_{1/2}$ and Cu(I) $2p_{1/2}$ (Fig. 7d).[70] Additionally, the C 1s spectra of BCNC-H shifted to higher binding energies, indicating strong chelation of Cu^{2+} ions with oxygen-containing functional groups (Fig. 7e and f).[70,71]

4. Conclusions and outlook

This study demonstrates a sustainable, cost-effective approach for producing BC by utilizing low-cost agro-industrial waste substrates such as molasses and cheese whey. The medium composed of molasses and cheese whey was optimized through response surface methodology. The optimized conditions yielded 6.17 ± 0.19 g L^{-1}, significantly outperforming traditional HS medium (0.9 ± 0.08 g L^{-1}). Post-synthesis modifications of BC *via* mild sulfuric acid hydrolysis and the Fenton reaction enabled the green production of carboxylated bacterial cellulose nanocrystals (BCNC-H), which exhibited reduced fiber diameter, increased surface negative charge, and a higher oxygen-to-carbon ratio. The carboxylation process enhanced the material's adsorption capabilities. BCNC-H demonstrated a maximum copper ion adsorption capacity of 164.17 ± 8.07 mg g^{-1}, representing a 173% increase compared to unmodified BC.

The integration of waste valorization, green chemical modification, and high-performance nanomaterials presents a compelling route toward circular and sustainable water treatment technologies. This approach not only reduces environmental pollution by repurposing industrial byproducts but also enables scalable production of high-performance adsorbents suitable for industrial and municipal water treatment. Future work will explore multi-metal adsorption capabilities, regeneration potential, and performance in dynamic flow systems to assess real-world applicability in wastewater remediation. Although adsorption kinetics and isotherm models were not studied, they are vital for understanding the adsorption mechanism and should be explored. Overall, the conversion of low-cost waste substrates into functionalized BCNC offers a sustainable, eco-friendly solution for heavy metal removal.

Author contributions

All authors contributed to the study's conception and design. Mohammad Sadegh Jafari wrote the manuscript and performed material preparation, data collection, and analysis. Samaneh Ghadami wrote the manuscript and performed material preparation, data collection, and analysis. Shobha Mantripragada performed and analyzed the XRD and XPS analysis. Kristen Dellinger assisted in editing and writing the manuscript. Jeffrey R. Alston assisted in editing and writing the manuscript.

Dennis LaJeunesse supervised the project. All authors read and approved the final manuscript.

Conflicts of interest

The authors have no relevant financial or non-financial interests to disclose.

Data availability

Supplementary information (SI). Within this file are the XRD data and the CCD experimental design table. See DOI: https://doi.org/10.1039/d5ma00725a.

All data supporting this study's findings are available within the article.

Acknowledgements

This work was performed at the JSNN, a member of the Southeastern Nanotechnology Infrastructure Corridor (SENIC) and National Nanotechnology Coordinated Infrastructure (NNCI), which is supported by the National Science Foundation (ECCS-1542174).

References

1 D. S. Tarahomi, S. P. Hosseini, A. Abbaspour, A. Jafari and S. M. Mousavi, Characterization and application of polysaccharides produced by Pseudomonas atacamensis M7D1 for chromium(III) removal from tannery effluent, *Int. J. Biol. Macromol.*, 2025, **298**, 139944, DOI: 10.1016/j.ijbiomac.2025.139944.

2 E. Khademian, E. Salehi, H. Sanaeepur, F. Galiano and A. Figoli, A systematic review on carbohydrate biopolymers for adsorptive remediation of copper ions from aqueous environments-part A: Classification and modification strategies, *Sci. Total Environ.*, 2020, **738**, 139829, DOI: 10.1016/j.scitotenv.2020.139829.

3 A. A. Aslam, S. U. Hassan, M. H. Saeed, O. Kokab, Z. Ali, M. S. Nazir, W. Siddiqi and A. A. Aslam, Cellulose-based adsorbent materials for water remediation: Harnessing their potential in heavy metal and dye removal, *J. Cleaner Prod.*, 2023, 138555, DOI: 10.1016/j.jclepro.2023.138555.

4 N. S. Topare and V. S. Wadgaonkar, A review on application of low-cost adsorbents for heavy metals removal from wastewater, *Mater. Today: Proc.*, 2023, **77**, 8–18, DOI: 10.1016/j.matpr.2022.08.450.

5 E. C. Emenike, A. G. Adeniyi, P. E. Omuku, K. C. Okwu and K. O. Iwuozor, Recent advances in nano-adsorbents for the sequestration of copper from water, *J. Water Process Eng.*, 2022, **47**, 102715, DOI: 10.1016/j.jwpe.2022.102715.

6 R. Luo, K. Zhang, Y. Qin, L. Xie, X. Chai, L. Zhang, G. Du, S. Ge, M. Rezakazemi and T. M. Aminabhavi, Amine-functionalized UiO-66 incorporated electrospun cellulose/chitosan porous nanofibrous membranes for removing copper ions, *Chem. Eng. J.*, 2024, **480**, 148077, DOI: 10.1016/j.cej.2023.148077.

7 X. Wang, X. Wang, W. Chen, J. Yuan and Q. Zhang, Adsorption of Cu(II) and Pb(II) in Aqueous Solution by Biochar Composites, *ACS Omega*, 2025, **10**(14), 13816–13828, DOI: 10.1021/acsomega.4c06837?urlappend=%3Fref%3DPDF&jav=VoR&rel=cite-as.

8 J. Kończyk, S. Żarska and W. Ciesielski, Adsorptive removal of Pb(II) ions from aqueous solutions by multi-walled carbon nanotubes functionalised by selenophosphoryl groups: Kinetic, mechanism, and thermodynamic studies, *Colloids Surf., A*, 2019, **575**, 271–282, DOI: 10.1016/j.colsurfa.2019.04.058.

9 T. W. Kurniawan, H. Sulistyarti, B. Rumhayati and A. Sabarudin, Cellulose nanocrystals (CNCs) and cellulose nanofibers (CNFs) as adsorbents of heavy metal ions, *J. Chem.*, 2023, **2023**(1), 5037027, DOI: 10.1155/2023/5037027.

10 D. Núñez, R. Cáceres, W. Ide, K. Varaprasad and P. Oyarzún, An ecofriendly nanocomposite of bacterial cellulose and hydroxyapatite efficiently removes lead from water, *Int. J. Biol. Macromol.*, 2020, **165**, 2711–2720, DOI: 10.1016/j.ijbiomac.2020.10.055.

11 D. K. Arserim-Uçar, F. Korel, L. Liu and K. L. Yam, Characterization of bacterial cellulose nanocrystals: Effect of acid treatments and neutralization, *Food Chem.*, 2021, **336**, 127597, DOI: 10.1016/j.foodchem.2020.127597.

12 P. Singhsa, R. Narain and H. Manuspiya, Bacterial cellulose nanocrystals (BCNC) preparation and characterization from three bacterial cellulose sources and development of functionalized BCNCs as nucleic acid delivery systems, *ACS Appl. Nano Mater.*, 2017, **1**(1), 209–221, DOI: 10.1021/acsanm.7b00105.

13 X. Jin, Z. Xiang, Q. Liu, Y. Chen and F. Lu, Polyethyleneimine-bacterial cellulose bioadsorbent for effective removal of copper and lead ions from aqueous solution, *Bioresour. Technol.*, 2017, **244**, 844–849, DOI: 10.1016/j.biortech.2017.08.072.

14 Z. He, H. Song, Y. Cui, W. Zhu, K. Du and S. Yao, Porous spherical cellulose carrier modified with polyethyleneimine and its adsorption for Cr(III) and Fe(III) from aqueous solutions, *Chin. J. Chem. Eng.*, 2014, **22**(9), 984–990, DOI: 10.1016/j.cjche.2014.07.001.

15 X.-M. Fan, H.-Y. Yu, D.-C. Wang, Z.-H. Mao, J. Yao and K. C. Tam, Facile and green synthesis of carboxylated cellulose nanocrystals as efficient adsorbents in wastewater treatments, *ACS Sustainable Chem. Eng.*, 2019, **7**(21), 18067–18075, DOI: 10.1021/acssuschemeng.9b05081.

16 S. Ye, H.-Y. Yu, D. Wang, J. Zhu and J. Gu, Green acid-free one-step hydrothermal ammonium persulfate oxidation of viscose fiber wastes to obtain carboxylated spherical cellulose nanocrystals for oil/water Pickering emulsion, *Cellulose*, 2018, **25**, 5139–5155, DOI: 10.1007/s10570-018-1917-x.

17 D. Li, Z. Chen, S. Zhang, Y. Xi, X. Liu, Y. Zhang, Y. Ding, S. Jia, Y. Xie and C. Zhong, Injectable copper ion cross-linked TEMPO-oxidized bacterial cellulose nanofiber hydrogels and their synergistic antimicrobial activity with glutathione, *Int.*

J. Biol. Macromol., 2025, 144287, DOI: 10.1016/j.ijbiomac.2025.144287.

18 P. Navya, V. Gayathri, D. Samanta and S. Sampath, Bacterial cellulose: A promising biopolymer with interesting properties and applications, *Int. J. Biol. Macromol.*, 2022, **220**, 435–461, DOI: 10.1016/j.ijbiomac.2022.08.056.

19 M. S. Jafari and P. Hejazi, Poly (3-hydroxybutyrate) production using supplemented corn-processing byproducts through Cupriavidus necator *via* solid-state fermentation: Cultivation on flask and bioreactor scale, *J. Biotechnol.*, 2024, **392**, 1–10, DOI: 10.1016/j.jbiotec.2024.06.013.

20 A. Karim and M. Aider, Sustainable valorization of whey by electroactivation technology for in situ isomerization of lactose into lactulose: Comparison between electroactivation and chemical processes at equivalent solution alkalinity, *ACS Omega*, 2020, **5**(14), 8380–8392, DOI: 10.1021/acsomega.0c00913.

21 R. J. Delgado-Macuil, B. Perez-Armendariz, G. A. Cardoso-Ugarte, S. E. M. Tolibia and A. C. Benítez-Rojas, Recent Biotechnological Applications of Whey: Review and Perspectives, *Fermentation*, 2025, **11**(4), 217, DOI: 10.3390/fermentation11040217.

22 M. Salari, M. S. Khiabani, R. R. Mokarram, B. Ghanbarzadeh and H. S. Kafil, Preparation and characterization of cellulose nanocrystals from bacterial cellulose produced in sugar beet molasses and cheese whey media, *Int. J. Biol. Macromol.*, 2019, **122**, 280–288, DOI: 10.1016/j.ijbiomac.2018.10.136.

23 M. S. Jafari, T. Khan, S. Mantripragada and D. R. LaJeunesse, Bacterial nanocellulose production: Improvement in productivity and properties *via* a sustainable medium, *Int. J. Biol. Macromol.*, 2024, 137607, DOI: 10.1016/j.ijbiomac.2024.137607.

24 S. Yadav and J. Pal, Optimisation of process parameters for lignocellulosic biomass degradation by Pseudomonas sp. using response surface methodology, *Int. J. Biol. Macromol.*, 2025, **309**, 142792, DOI: 10.1016/j.ijbiomac.2025.142792.

25 M. Arshadi and S. Mousavi, Multi-objective optimization of heavy metals bioleaching from discarded mobile phone PCBs: simultaneous Cu and Ni recovery using Acidithiobacillus ferrooxidans, *Sep. Purif. Technol.*, 2015, **147**, 210–219, DOI: 10.1016/j.seppur.2015.04.020.

26 D. C. Montgomery, *Design and analysis of experiments*, John Wiley & Sons, 2017.

27 M. DuBois, K. A. Gilles, J. K. Hamilton, Pt Rebers and F. Smith, Colorimetric method for determination of sugars and related substances, *Anal. Chem.*, 1956, **28**(3), 350–356.

28 G. L. Miller, Use of dinitrosalicylic acid reagent for determination of reducing sugar, *Anal. Chem.*, 1959, **31**(3), 426–428.

29 H. Yan, X. Chen, H. Song, J. Li, Y. Feng, Z. Shi, X. Wang and Q. Lin, Synthesis of bacterial cellulose and bacterial cellulose nanocrystals for their applications in the stabilization of olive oil pickering emulsion, *Food Hydrocolloids*, 2017, **72**, 127–135, DOI: 10.1016/j.foodhyd.2017.05.044.

30 O. Peiravi-Rivash, M. Mashreghi, O. Baigenzhenov and A. Hosseini-Bandegharaei, Producing bacterial nano-cellulose and keratin from wastes to synthesize keratin/cellulose nanobiocomposite for removal of dyes and heavy metal ions from waters and wastewaters, *Colloids Surf., A*, 2023, **656**, 130355, DOI: 10.1016/j.colsurfa.2022.130355.

31 L. Segal, J. J. Creely, A. Martin Jr and C. Conrad, An empirical method for estimating the degree of crystallinity of native cellulose using the X-ray diffractometer, *Text. Res. J.*, 1959, **29**(10), 786–794, DOI: 10.1177/004051755902901003.

32 A. Patterson, The Scherrer formula for X-ray particle size determination, *Phys. Rev.*, 1939, **56**(10), 978, DOI: 10.1103/PhysRev.56.978.

33 A. C. Rodrigues, A. I. Fontão, A. Coelho, M. Leal, F. A. S. da Silva, Y. Wan, F. Dourado and M. Gama, Response surface statistical optimization of bacterial nanocellulose fermentation in static culture using a low-cost medium, *New Biotechnol.*, 2019, **49**, 19–27, DOI: 10.1016/j.nbt.2018.12.002.

34 Z. Peng, Z. Lv, J. Liu, Y. Wang, T. Zhang, Y. Xie, S. Jia, B. Xin and C. Zhong, Engineering PTS-based glucose metabolism for efficient biosynthesis of bacterial cellulose by Komagataeibacter xylinus, *Carbohydr. Polym.*, 2024, **343**, 122459, DOI: 10.1016/j.carbpol.2024.122459.

35 H. Zhang, C. Chen, C. Zhu and D. Sun, Production of bacterial cellulose by *Acetobacter xylinum*: effects of carbon/nitrogen-ratio on cell growth and metabolite production, *Cellul. Chem. Technol.*, 2016, **50**, 997–1003.

36 V. Revin, E. Liyaskina, M. Nazarkina, A. Bogatyreva and M. Shchankin, Cost-effective production of bacterial cellulose using acidic food industry by-products, *Braz. J. Microbiol.*, 2018, **49**(suppl 1), 151–159, DOI: 10.1016/j.bjm.2017.12.012.

37 M. Gullo, G. Zanichelli, E. Verzelloni, F. Lemmetti and P. Giudici, Feasible acetic acid fermentations of alcoholic and sugary substrates in combined operation mode, *Process Biochem.*, 2016, **51**(9), 1129–1139, DOI: 10.1016/j.procbio.2016.05.018.

38 Y. S. Tseng, R. R. Singhania, A.-C. Cheng, C.-W. Chen, C.-D. Dong and A. K. Patel, Removal of heavy metal vanadium from aqueous solution by nanocellulose produced from Komagataeibacter europaeus employing pineapple waste as carbon source, *Bioresour. Technol.*, 2023, **369**, 128411, DOI: 10.1016/j.biortech.2022.128411.

39 H. Lima, E. Nascimento, F. Andrade, A. Brígida, M. D. F. Borges, A. Cassales, C. Muniz, M. Souza, J. Morais and M. D. F. Rosa, Bacterial cellulose production by Komagataeibacter hansenii ATCC 23769 using sisal juice-an agroindustry waste, *Braz. J. Chem. Eng.*, 2017, **34**, 671–680, DOI: 10.1590/0104-6632.20170343s20150514.

40 P. Sharma, R. Sharma, A. Yadav and N. K. Aggarwal, Sustainable and cost-effective production of bacterial cellulose by using rice straw hydrolysate: a response surface approach, *Braz. J. Microbiol.*, 2025, 1–11, DOI: 10.1007/s42770-025-01692-z.

41 H. El-Gendi, A. Salama, E. M. El-Fakharany and A. K. Saleh, Optimization of bacterial cellulose production from prickly pear peels and its ex situ impregnation with fruit

byproducts for antimicrobial and strawberry packaging applications, *Carbohydr. Polym.*, 2023, **302**, 120383, DOI: 10.1016/j.carbpol.2022.120383.

42 E. F. Souza, M. R. Furtado, C. W. Carvalho, O. Freitas-Silva and L. M. Gottschalk, Production and characterization of *Gluconacetobacter xylinus* bacterial cellulose using cashew apple juice and soybean molasses, *Int. J. Biol. Macromol.*, 2020, **146**, 285–289, DOI: 10.1016/j.ijbiomac.2019.12.180.

43 E. Bialik, B. R. Stenqvist, Y. Fang, Å. Östlund, I. Furó, B. R. Lindman, M. Lund and D. Bernin, Ionization of cellobiose in aqueous alkali and the mechanism of cellulose dissolution, *J. Phys. Chem. Lett.*, 2016, **7**(24), 5044–5048, DOI: 10.1021/acs.jpclett.6b02346.

44 W. R. Warren and D. R. LaJeunesse, Characterization of hydrothermal deposition of copper oxide nanoleaves on never-dried bacterial cellulose, *Polymers*, 2019, **11**(11), 1762, DOI: 10.3390/polym11111762.

45 P. Tolvanen, P. Mäki-Arvela, A. Sorokin, T. Salmi and D. Y. Murzin, Kinetics of starch oxidation using hydrogen peroxide as an environmentally friendly oxidant and an iron complex as a catalyst, *Chem. Eng. J.*, 2009, **154**(1–3), 52–59, DOI: 10.1016/j.cej.2009.02.001.

46 W.-S. Chang and H.-H. Chen, Physical properties of bacterial cellulose composites for wound dressings, *Food Hydrocolloids*, 2016, **53**, 75–83, DOI: 10.1016/j.foodhyd.2014.12.009.

47 P. Liu, K. Oksman and A. P. Mathew, Surface adsorption and self-assembly of Cu(II) ions on TEMPO-oxidized cellulose nanofibers in aqueous media, *J. Colloid Interface Sci.*, 2016, **464**, 175–182, DOI: 10.1016/j.jcis.2015.11.033.

48 P. Jacek, F. A. S. da Silva, F. Dourado, S. Bielecki and M. Gama, Optimization and characterization of bacterial nanocellulose produced by Komagataeibacter rhaeticus K3, *Carbohydr. Polym. Technol. Appl.*, 2021, **2**, 100022, DOI: 10.1016/j.carpta.2020.100022.

49 M. U. A. Khan, G. M. Stojanovic, R. Hassan, T. J. S. Anand, M. Al-Ejji and A. Hasan, Role of graphene oxide in bacterial cellulose–gelatin hydrogels for wound dressing applications, *ACS Omega*, 2023, **8**(18), 15909–15919, DOI: 10.1021/acsomega.2c07279?urlappend=%3Fref%3DPDF&jav=VoR&rel=cite-as.

50 S. Pal, R. Nisi, M. Stoppa and A. Licciulli, Silver-functionalized bacterial cellulose as antibacterial membrane for wound-healing applications, *ACS Omega*, 2017, **2**(7), 3632–3639, DOI: 10.1021/acsomega.7b00442.

51 H. Yan, X. Chen, J. Li, Y. Feng, Z. Shi, X. Wang and Q. Lin, Synthesis of alginate derivative via the Ugi reaction and its characterization, *Carbohydr. Polym.*, 2016, **136**, 757–763, DOI: 10.1016/j.carbpol.2015.09.104.

52 N. O. Pinto, A. I. Bourbon, D. Martins, A. Pereira, M. A. Cerqueira, L. Pastrana, M. Gama, H. M. Azeredo, M. F. Rosa and C. Gonçalves, Bacterial cellulose nanocrystals or nanofibrils as Pickering stabilizers in low-oil emulsions: A comparative study, *Food Hydrocolloids*, 2024, **157**, 110427, DOI: 10.1016/j.foodhyd.2024.110427.

53 J. Nam, Y. Hyun, S. Oh, J. Park, H.-J. Jin and H. W. Kwak, Effect of cross-linkable bacterial cellulose nanocrystals on the physicochemical properties of silk sericin films, *Polym. Test.*, 2021, **97**, 107161, DOI: 10.1016/j.polymertesting.2021.107161.

54 X. Yang, Y. Wan, Y. Zheng, F. He, Z. Yu, J. Huang, H. Wang, Y. S. Ok, Y. Jiang and B. Gao, Surface functional groups of carbon-based adsorbents and their roles in the removal of heavy metals from aqueous solutions: a critical review, *Chem. Eng. J.*, 2019, **366**, 608–621, DOI: 10.1016/j.cej.2019.02.119.

55 F. Netzer, A. P. Manian, T. Bechtold and T. Pham, The role of carboxyl and cationic groups in low-level cationised cellulose fibres investigated by zeta potential and sorption studies, *Cellulose*, 2024, **31**(14), 8501–8517, DOI: 10.1007/s10570-024-06132-z.

56 R. Koshani and T. G. van de Ven, Carboxylated cellulose nanocrystals developed by Cu-assisted H2O2 oxidation as green nanocarriers for efficient lysozyme immobilization, *J. Agric. Food Chem.*, 2020, **68**(21), 5938–5950, DOI: 10.1021/acs.jafc.0c00538?ref=pdf.

57 B. Jia, X. Chen, Y. Shen, Z. Li, X. Ma and H.-Y. Yu, Two-response surface design optimization of carboxylated CNCs with super high thermal stability and dye removal capability, *Carbohydr. Polym.*, 2024, **342**, 122395, DOI: 10.1016/j.carbpol.2024.122395.

58 S. Li, J. Hao, S. Yang, Y. Wang and Y. Li, Alginate-based adsorbents with adjustable slit-shaped pore structure for selective removal of copper ions, *Int. J. Biol. Macromol.*, 2024, **267**, 131484, DOI: 10.1016/j.ijbiomac.2024.131484.

59 S. Chen, Y. Zou, Z. Yan, W. Shen, S. Shi, X. Zhang and H. Wang, Carboxymethylated-bacterial cellulose for copper and lead ion removal, *J. Hazard. Mater.*, 2009, **161**(2–3), 1355–1359, DOI: 10.1016/j.jhazmat.2008.04.098.

60 M. Omidinasab, N. Rahbar, M. Ahmadi, B. Kakavandi, F. Ghanbari, G. Z. Kyzas, S. S. Martinez and N. Jaafarzadeh, Removal of vanadium and palladium ions by adsorption onto magnetic chitosan nanoparticles, *Environ. Sci. Pollut. Res.*, 2018, **25**, 34262–34276, DOI: 10.1007/s11356-018-3137-1.

61 J. Kończyk, K. Kluziak and D. Kołodyńska, Adsorption of vanadium (V) ions from the aqueous solutions on different biomass-derived biochars, *J. Environ. Manage.*, 2022, **313**, 114958, DOI: 10.1016/j.jenvman.2022.114958.

62 W. Shen, S. Chen, S. Shi, X. Li, X. Zhang, W. Hu and H. Wang, Adsorption of Cu(II) and Pb(II) onto diethylenetriamine-bacterial cellulose, *Carbohydr. Polym.*, 2009, **75**(1), 110–114, DOI: 10.1016/j.carbpol.2008.07.006.

63 R. Ding, S. Hu, M. Xu, Q. Hu, S. Jiang, K. Xu, P.-L. Tremblay and T. Zhang, The facile and controllable synthesis of a bacterial cellulose/polyhydroxybutyrate composite by co-culturing *Gluconacetobacter xylinus* and Ralstonia eutropha, *Carbohydr. Polym.*, 2021, **252**, 117137, DOI: 10.1016/j.carbpol.2020.117137.

64 P. Liu, P. F. Borrell, M. Božič, V. Kokol, K. Oksman and A. P. Mathew, Nanocelluloses and their phosphorylated derivatives for selective adsorption of Ag +, Cu2+ and Fe3+ from industrial effluents, *J. Hazard. Mater.*, 2015, **294**, 177–185, DOI: 10.1016/j.jhazmat.2015.04.001.

65 P. Phuengphai, T. Singjanusong, N. Kheangkhun and A. Wattanakornsiri, Removal of copper(II) from aqueous solution using chemically modified fruit peels as efficient low-cost biosorbents, *Water Sci. Eng.*, 2021, **14**(4), 286–294, DOI: **10.1016/j.wse.2021.08.003**.

66 A. Solanki, Z. Ahamad and V. Gupta, Upcycling waste biomass: Alkali-modified watermelon rind as a lignocellulosic bioadsorbent for copper ion removal, *Ind. Crops Prod.*, 2025, **224**, 120340, DOI: **10.1016/j.indcrop.2024.120340**.

67 I. S. Mir, A. Riaz, J. S. Roy, J. Fréchette, S. Morency, O. P. Gomes, L. F. Dumée, J. Greener and Y. Messaddeq, Removal of cadmium and chromium heavy metals from aqueous medium using composite bacterial cellulose membrane, *Chem. Eng. J.*, 2024, **490**, 151665, DOI: **10.1016/j.cej.2024.151665**.

68 C. Lai, L. Sheng, S. Liao, T. Xi and Z. Zhang, Surface characterization of TEMPO-oxidized bacterial cellulose, *Surf. Interface Anal.*, 2013, **45**(11–12), 1673–1679, DOI: **10.1002/sia.5306**.

69 N. F. Vasconcelos, F. K. Andrade, L. D. A. P. Vieira, R. S. Vieira, J. M. Vaz, P. Chevallier, D. Mantovani, M. D. F. Borges and M. D. F. Rosa, Oxidized bacterial cellulose membrane as support for enzyme immobilization: properties and morphological features, *Cellulose*, 2020, **27**(6), 3055–3083, DOI: **10.1007/s10570-020-02966-5**.

70 Y. Qin, B. Chai, Y. Sun, X. Zhang, G. Fan and G. Song, Amino-functionalized cellulose composite for efficient simultaneous adsorption of tetracycline and copper ions: Performance, mechanism and DFT study, *Carbohydr. Polym.*, 2024, **332**, 121935, DOI: **10.1016/j.carbpol.2024.121935**.

71 J. Guo, H. Tian and J. He, Integration of CuS nanoparticles and cellulose fibers towards fast, selective and efficient capture and separation of mercury ions, *Chem. Eng. J.*, 2021, **408**, 127336, DOI: **10.1016/j.cej.2020.127336**.